



# Periodic Modeling and Effect of Design Parameters of Semitransparent Photovoltaic Thermal Trombe Wall (SPVT-TW) with Air Duct

Firehun Taffesse<sup>a\*</sup>, Neha Dimri<sup>a</sup>, Arvind Tiwari<sup>b</sup>, Emran Khan<sup>c</sup>, G. N. Tiwari<sup>c</sup> and T.S. Bhatti<sup>a</sup>

<sup>a</sup>Centre for Energy Studies, Indian Institute of Technology Delhi, Hauz Khas, New Delhi, India

<sup>b</sup>Department of Electrical Engineering, College of Engineering, Qassim University, Buraidah, Saudi Arabia

<sup>c</sup>Department of Mechanical Engineering, Faculty of Engineering and Technology, Jamia Millia Islamia, New Delhi, India

**Abstract**— Trombe wall is one of the unique features in passive solar house development, which facilitates heat storage. A mathematical model of semitransparent photovoltaic thermal Trombe wall (SPVT-TW) with air ducts (or vents) has been derived in this paper, for a single room of 30 m<sup>2</sup> dimension, for winter season of New Delhi, India. The model is derived considering the energy balance equations taking into account the periodic nature of solar radiation and ambient temperature. Further, the effect of several parameters namely, thickness of wall, mass flow rate, packing factor, absorptivity and transmittivity of PV module on room air temperature and thermal stability have been examined. The performance of vented SPVT-TW has been compared with SPVT-TW without vent. The results illustrate that the thickness of the room should be 0.3 m, with a corresponding thermal load leveling of 0.0038, for vented SPVT-TW, from a thermal stability point of view. Also, the room air temperature of 45 °C can be reached in case of vented SPVT-TW, which is higher than SPVT-TW without vent.

**Keywords**— *Periodic modeling, heating the room, Trombe wall, Photovoltaic thermal (PVT)*

## I. INTRODUCTION

Passive solar heating can be utilized for maintaining a pleasant temperature within a building without the use of conventional energy sources. There are a wide range of studies and investigations pertaining to Trombe wall for different seasons and climatic conditions. Smolec and Thomas (1991) calculated the temperature distribution in Trombe wall theoretically, using PASOLE model and compared the results with experimental data. Mansour et. al.(1991) studied the convective laminar heat transfer between the Trombe wall's channel surfaces and developed a mathematical model for temperature profiles, pressure defects and velocity using new approximate methods. Photovoltaic Trombe wall is not only

used for thermal heating, but also for thermal cooling of buildings. Gan (1998) studied the cooling of building in summer condition using Trombe wall. They used computational fluid dynamics with renormalization group k- $\epsilon$  turbulence model to predict the flow rate and buoyant flow. Further, they investigated the effects of various parameters such as wall height, wall insulation, wall and glazing separation and glazing type. Finally, it was concluded that the inner surface of a Trombe wall should be insulated to allow for cooling as well as to prevent overheating of air due to heat radiation from inner portion of the wall. Furthermore, the design parameters of photovoltaic module affect thermal utilization as well as electrical efficiency. Jie et al. (2007) have studied a model of PV glass panel and of Photovoltaic Trombe wall (PV-TW). The electrical performance and temperature distribution of PV-TW was obtained. They concluded that the temperature difference between the components in the presence and absence of PV glass panel reaches the highest value of 10.6 °C and the electrical efficiency increases by 10%. Jiang et. al. (2008) have discussed the effects of photovoltaic coverage ratio. As the coverage ratio increases, the electrical energy output and total efficiency of PV-TW increases, however the thermal efficiency and interior temperature decreases. Koyunbaba and Yilmaz (2012) examined different arrangements of single glass, double glass and a Si-semitransparent PV module integrated with Trombe wall in Izmir, Turkey. For transient analysis, a two-dimensional model using computational fluid dynamics (CFD) was developed. They compared the results of simulation with the experimental results and concluded them to be in a good agreement. Rabani et. al (2015) evaluated the energy generated and heating comfort for Yazd city (Iran) desert climate considering winter operation. They implemented a new design of Trombe wall to gather solar

radiation from three different directions (South, East and West), so that the absorbing surface of the wall is subjected to the solar radiation throughout daytime. The temperature of the room was kept within 15 °C to 30 °C and stored hourly energy attained a maximum value of 5800 kJ/h. Irshad et. al. (2015) assessed a single room building's performance with PV-TW using TRNSYS software. Also, they discussed the effect of air velocity for three types of glazing namely, single glazing, double glazing and double glazing with Argon gas. Taffesse et. al. (2016) performed periodic modeling of SPVT-TW without air ducts. Also, they studied the role of parameters such as absorptivity, packing factor and thickness, and evaluated thermal load leveling, hourly room air temperature and decrement factor for the climatic condition of New Delhi, India. The optimum thickness of the wall was computed to be 0.3m to 0.4 m, based on theoretical calculations. The aim of this research work is to modify the SPVT-TW proposed by Taffesse et. al. (2016) by incorporating air ducts/vents. A periodic model of vented SPVT-TW has been developed and the results obtained from vented SPVT-TW are compared with SPVT-TW without vent (Taffesse et. al., 2016).

## II. DESCRIPTION OF SPVT-TW WITH AIR DUCT

Trombe wall is a passive solar heating system and is used for space heating applications. Its performance depends on the materials used, the orientation with respect to the sun and the vents' design. In this case, a semitransparent PV module is integrated with a south oriented Trombe wall in a room of dimension 30 m<sup>2</sup>. An air duct is present between the PV module and Trombe wall with a fan, as shown in Fig. 1. In case of a non-vented arrangement (Taffesse et. al., 2016), the heat from solar radiation is transmitted into the room through indirect gain only. This vented arrangement will provide heat into the room in two ways namely, direct gain and indirect gain. Direct gain, through the circulation of hot air with the help of fan, provides heat at the top, whereas indirect gain, through the heat energy propagated across the Trombe wall by conduction, heats the room. Thus, the room is heated and the thermal comfort is improved. Further, the electrical efficiency of the integrated PV module will increase as a result of air circulation through ventilation.

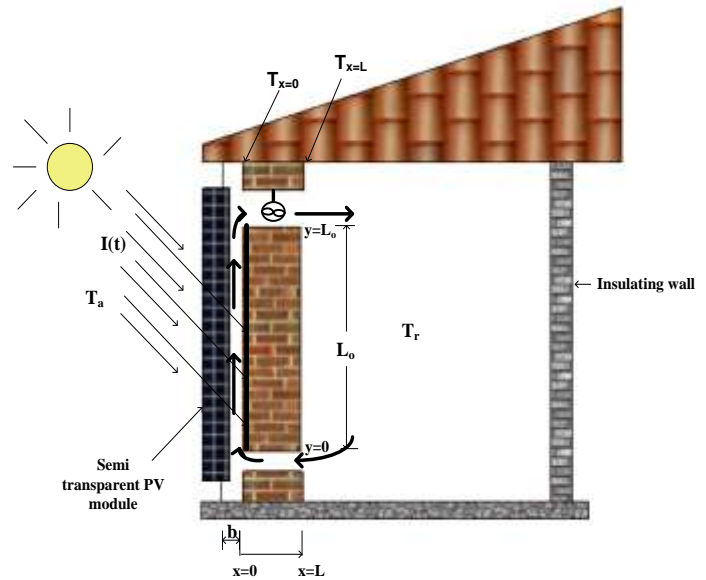


Fig. 1. Schematic diagram of SPVT-TW with air duct/vent.

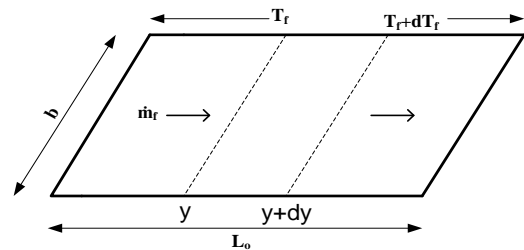


Fig. 2. Cross sectional view of air flow through the duct/vent.

## III. MATHEMATICAL MODELING OF SPVT-TW WITH AIR DUCT (VENT)

The following assumptions have been made in deriving the mathematical model of SPVT-TW with vent:

- One-dimensional heat flow is considered.
- Thermal losses through sidewalls and roof are negligible.
- Physical and thermal properties of air are constant, for operating temperature range.
- Flow is laminar and incompressible.
- The system is under periodic condition.
- No ventilation has been considered.

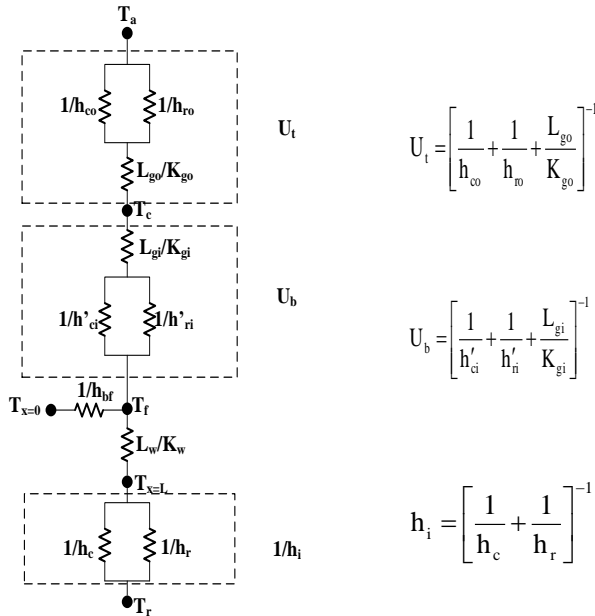


Fig.3. Thermal circuit diagram of SPVT-TW with air duct/vent

Based on these assumptions, the energy balance equations considering an elemental area, 'bdy' (Fig. 2), for each component of SPVT-TW with air duct/vent can be written next. By considering Figs. 2 and 3, the energy balance equations are:

**For semitransparent PV module:**

$$\tau_g \alpha_c \beta I(t) A_m = U_t (T_c - T_a) A_m + U_b (T_c - T_f) A_m + \eta_m \beta I(t) A_m$$

or

$$\tau_g \alpha_c \beta I(t) = U_t (T_c - T_a) + U_b (T_c - T_f) + \eta_m \beta I(t) \quad (1)$$

where  $\eta_m = \tau_g \eta_{co} [1 - \beta_o (T_c - T_o)]$

Substituting  $\eta_m$  from above in Eq. (1), we get

$$(\alpha \tau)_{eff} I(t) + U_t T_a + U_b T_f = (U_{tb} - PF_1 I(t)) T_c \quad (2)$$

Where

$$(\alpha \tau)_{eff} = \tau_g \alpha_c \beta - \tau_g \eta_{co} \beta (1 + \beta_o T_o), U_{tb} = U_t + U_b \text{ and } PF_1 = \tau_g \eta_{co} \beta \beta_o$$

$$U_t = \left[ \frac{L_g}{K_g} + \frac{1}{h_o} \right]^{-1}, h_o = 5.7 + 3.8 V_a, V_a = 0 \text{ m/s}$$

and

$$U_b = \left[ \frac{L_g}{K_g} + \frac{1}{h_i} \right]^{-1}, h_i = 2.8 + 3 v_a, v_a = 0 \text{ m/s}$$

**For Trombe wall at x=0 (Fig. 1):**

$$\tau_g^2 \alpha_{bb} (1 - \beta) I(t) A_m + h_{bf} (T_f - T|_{x=0}) A_m = \left( -k \frac{\partial T}{\partial x} \Big|_{x=0} \right) A_m$$

or

$$\tau_g^2 \alpha_{bb} (1 - \beta) I(t) + h_{bf} (T_f - T|_{x=0}) = \left( -k \frac{\partial T}{\partial x} \Big|_{x=0} \right) \quad (3)$$

**For Trombe wall at x=L (Fig. 1):**

$$-k \frac{\partial T}{\partial x} \Big|_{x=L} = h_i (T|_{x=L} - T_r) \quad (4)$$

**For non-air conditioning room:**

Energy balance equation for room air is as follows:

$$M_a C_a \frac{dT_r}{dt} = h_i (T|_{x=L} - T_r) A_r + \dot{Q}_{in} = \dot{m}_f C_f (T_f - T_r) \quad (5)$$

where  $\dot{Q}_{in}$  is the heat gain through the upper vent/duct.

The energy balance equation for flowing fluid (air) in

$$\dot{m}_f c_f \frac{dT_f}{dy} dy = U_b (T_c - T_f) b dy + h_{bf} (T|_{x=0} - T_f) b dy$$

or

$$\dot{m}_f c_f \frac{dT_f}{dy} = U_b (T_c - T_f) b + h_{bf} (T|_{x=0} - T_f) b \quad (6)$$

Now,  $I(t)$  and  $T_a$  can be expressed in terms of Fourier series, due to periodic nature, as:

$$I(t) = I_o + \text{real} \sum_{n=1}^{\infty} I_n e^{-i\psi_n} e^{in\omega t} \quad (7a)$$

and,

$$T_a = T_{ao} + \text{real} \sum_{n=1}^{\infty} T_{an} e^{-i\sigma_n} e^{in\omega t} \quad (7b)$$

where  $I_o, I_n, T_{ao}, T_{an}, \psi_n$ , and  $\sigma_n$  are Fourier coefficients and are evaluated for known values of  $I(t)$  and  $T_a$  (Fig. 4).

Furthermore, since  $T_a$  and  $I(t)$  are periodic in nature,  $T_c, T, T_r$  and  $T_f$  can be expressed as:



$$T_c = T_{co} + \text{real} \sum_{n=1}^6 T_{cn} e^{inwt} \quad (8)$$

$$T = Ax + B + \text{real} \sum_{n=1}^6 (C_n e^{-\beta_n x} + D_n e^{\beta_n x}) e^{inwt} \quad (9)$$

$$T_r = T_{ro} + \text{real} \sum_{n=1}^6 T_{rn} e^{inwt} \quad (10)$$

$$T_f = T_{fo} + \text{real} \sum_{n=1}^6 T_{fn} e^{inwt} \quad (11)$$

Substituting Eqs. ((7) - (11)) in Eqs. (2) - (6), we get

$$(\alpha\tau)_{\text{eff}} [I_o + \text{real} \sum_{n=1}^6 I_n e^{-i\omega_n} e^{inwt}] + U_t [T_{ao} + \text{real} \sum_{n=1}^6 T_{an} e^{-i\sigma_n} e^{inwt}] + U_b [T_{fo} + \text{real} \sum_{n=1}^6 T_{fn} e^{inwt}] = [U_{tb} - PF_1 I_o + \text{real} \sum_{n=1}^6 I_n e^{-i\omega_n} e^{inwt}] [T_{co} + \text{real} \sum_{n=1}^6 T_{cn} e^{inwt}] \quad (12)$$

$$(\alpha\tau)'_{\text{eff}} [I_o + \text{real} \sum_{n=1}^6 I_n e^{-i\omega_n} e^{inwt}] + h_{bf} [T_{fo} + \text{real} \sum_{n=1}^6 T_{fn} e^{inwt} - B - \text{real} \sum_{n=1}^6 (C_n + D_n) e^{inwt}] = -K[A + \text{real} \sum_{n=1}^6 (-\beta_n C_n + \beta_n D_n) e^{inwt}] \quad (13)$$

$$-K[A + \text{real} \sum_{n=1}^6 (-\beta_n C_n e^{-\beta_n L} + \beta_n D_n e^{\beta_n L}) e^{inwt}] = h_i [AL + B + \text{real} \sum_{n=1}^6 (C_n e^{-\beta_n L} + D_n e^{\beta_n L}) e^{inwt} - T_{ro} - \text{real} \sum_{n=1}^6 T_{rn} e^{inwt}] \quad (14)$$

$$M_a C_a [\text{real} \sum_{n=1}^6 inw T_{fn} e^{inwt}] = A_r h_i [AL + B + \text{real} \sum_{n=1}^6 (C_n e^{-\beta_n L} + D_n e^{\beta_n L}) e^{inwt} - T_{ro} - \text{real} \sum_{n=1}^6 T_{rn} e^{inwt}] + \dot{m}_a c_a [T_{fo} + \text{real} \sum_{n=1}^6 T_{fn} e^{inwt} - T_{ro} - \text{real} \sum_{n=1}^6 T_{rn} e^{inwt}] \quad (15)$$

$$\dot{m}_a c_a [T_{fo} + \text{real} \sum_{n=1}^6 T_{fn} e^{inwt}] = U_b (T_{co} + \text{real} \sum_{n=1}^6 T_{cn} e^{inwt} - T_{fo}) - \text{real} \sum_{n=1}^6 T_{fn} e^{inwt} b + h_{bf} (B + \text{real} \sum_{n=1}^6 (C_n + D_n) e^{inwt} - T_{fo} - \text{real} \sum_{n=1}^6 T_{fn} e^{inwt}) b \quad (16)$$

Next, we consider the Eqs. (12) - (16) for time-independent portion and time-dependent portion separately.

### Time-independent portion

The time-independent portion of Eqs. (12) - (16) are:

$$(\alpha\tau)_{\text{eff}} I_o + U_t T_{ao} + U_b T_{fo} = U_{tb} T_{co} - PF_1 I_o T_{co} \quad (17)$$

$$(\alpha\tau)'_{\text{eff}} I_o + h_{bf} (T_{fo} - B) = -KA \quad (18)$$

$$-KA = h_i [AL + B - T_{ro}] \quad (19)$$

$$0 = A_r h_i [AL + B - T_{ro}] + \dot{m}_a c_a [T_{fo} - T_{ro}] \quad (20)$$

$$\dot{m}_a c_a \frac{dT_{fo}}{dy} = b U_b (T_{co} - T_{fo}) + b h_{bf} (B - T_{fo}) \quad (21)$$

Eq. (21) can be solved for  $T_{fo}$  and the average value of flowing fluid (air) temperature using initial condition  $T_{fo}|_{x=0} = T_{ro}$  as follows:

$$\bar{T}_{fo} = \frac{1}{L_o} \int_0^{L_o} T_{fo} dx = \frac{U_b T_{co} + h_{bf} B}{U_{tT}} \left[ 1 - \left[ \frac{1 - e^{-q_u L_o}}{q_u L_o} \right] \right] + T_{ro} \left[ \frac{1 - e^{-q_u L_o}}{q_u L_o} \right]$$

$$\bar{T}_{fo} = g_{12} \left[ \frac{U_b T_{co} + h_{bf} B}{U_{tT}} \right] + g_{13} T_{ro} \quad (22)$$

where  $g_{12} = 1 - \left( \frac{1 - e^{-q_u L_o}}{q_u L_o} \right)$  and  $g_{13} = \frac{1 - e^{-q_u L_o}}{q_u L_o}$

Substituting Eq. (22) in Eqs. ((17) - (20)), the time-independent equations are simplified

$$-\frac{U_b h_{bf}}{U_{tT}} g_{12} B + (U_{tb} - PF_1 I_o - \frac{U_b^2}{U_{tT}} g_{12}) T_{co} - U_b g_{13} T_{ro} = (\alpha\tau)_{\text{eff}} I_o + U_t T_{ao} \quad (23)$$

$$(\alpha\tau)'_{\text{eff}} I_o + \frac{h_{bf} U_b g_{12}}{U_{tT}} T_{co} + \frac{g_{12} h_{bf}^2}{U_{tT}} B + h_{bf} g_{13} T_{ro} - h_{bf} B = -KA \quad (24)$$

$$-KA = h_i [AL + B - T_{ro}] \quad (25)$$

$$0 = A_r h_i LA + (A_r h_i + \frac{\dot{m}_a c_a h_{bf} g_{12}}{U_{tT}}) B + \frac{\dot{m}_a c_a U_b}{U_{tT}} T_{co} - (A_r h_i - \dot{m}_a c_a g_{13} + \dot{m}_a c_a) T_{ro} \quad (26)$$

Eqs. (23) - (26) can be arranged in a matrix form as:



$$\begin{bmatrix} 0 & -\frac{U_b h_{bf} g_{12}}{U_{tr}} & U_{tb} - PF_1 I_o - \frac{U_b^2 g_{12}}{U_{tr}} & -U_b g_{13} \\ -K & h_{bf} - \frac{g_{12} h_{bf}^2}{U_{tr}} & \frac{-h_{bf} U_b g_{12}}{U_{tr}} & -h_{bf} g_{13} \\ h_i L + K & h_i & 0 & -h_i \\ A_r h_i L & A_r h_i + \frac{\dot{m}_a c_a h_{bf} g_{12}}{U_{tr}} & \frac{\dot{m}_a c_a h_{bf} g_{12}}{U_{tr}} & -(A_r h_i - \dot{m}_a c_a g_{13} + \dot{m}_a c_a) \end{bmatrix} \begin{bmatrix} A \\ B \\ T_{co} \\ T_{ro} \end{bmatrix} = \begin{bmatrix} (\alpha\tau)_{eff} I_o + U_t T_{ao} \\ (\alpha\tau)'_{eff} I_o \\ 0 \\ 0 \end{bmatrix} \quad (27)$$

• Time-dependent portion

Similarly, a matrix for time-dependent portion can be written as:

$$\begin{bmatrix} \frac{U_b h_{bf} g_{12}}{U_{tr}} & \frac{U_b h_{bf} g_{12}}{U_{tr}} & U_{tb} - PF_1 I_o - PF_1 I_n e^{-i\psi_n} - \frac{U_b^2 g_{12}}{U_{tr}} & -U_b g_{13} \\ K\beta_n + h_{bf} + \frac{h_{bf}^2 g_{12}}{U_{tr}} & -(K\beta_n - h_{bf} + \frac{h_{bf}^2 g_{12}}{U_{tr}}) & -\frac{g_{12} h_{bf} U_b}{U_{tr}} & -h_{bf} g_{13} \\ K\beta_n e^{-\beta_n L} - h_i & -(K\beta_n e^{\beta_n L} + h_i) & 0 & h_i \\ A_r h_i e^{-\beta_n L} + \frac{\dot{m}_a c_a h_{bf} g_{12}}{U_{tr}} & A_r h_i e^{\beta_n L} + \frac{\dot{m}_a c_a h_{bf} g_{12}}{U_{tr}} & 0 & -(A_r h_i - \dot{m}_a c_a g_{13} + \dot{m}_a c_a + M_a c_a inw) \end{bmatrix}$$

$$\begin{bmatrix} C_n \\ D_n \\ T_{cn} \\ T_{m} \end{bmatrix} = \begin{bmatrix} G_1 \\ G_2 \\ 0 \\ 0 \end{bmatrix} \quad (28)$$

where

$$G_1 = (\alpha\tau)_{eff} I_n e^{-i\psi_n} + U_t T_{an} e^{-i\psi_n} + PF_1 T_{co} I_n e^{-i\psi_n}$$

$$G_2 = -(\alpha\tau)'_{eff} I_n e^{-i\psi_n}$$

$$(\alpha\tau)'_{eff} = \tau_g^2 \alpha_{bb} (1 - \beta)$$

$$PF_1 = \tau_g \beta \beta_o \eta_{co}$$

$$(\alpha\tau)_{eff} = \tau_g \alpha_c \beta - \tau_g \beta \eta_{co} [1 + \beta_o T_o]$$

Using matrices in Eqs. (27) and (28), all the unknown constants for time-independent portion and time-dependent portion can be evaluated. Subsequently,  $T_c$ ,  $T_r$ , and  $T_f$  can be obtained from Eqs. (8), (10) and (11), respectively.

Further,  $T|_{x=0}$  and  $T|_{x=L}$  can be obtained as follows:

$$T|_{x=0} = B + \text{real} \sum_{n=1}^{\infty} (C_n + D_n) e^{in\omega t} \quad (29a)$$

$$T|_{x=L} = AL + B + \text{real} \sum_{n=1}^{\infty} (C_n e^{-\beta_n L} + D_n e^{\beta_n L}) e^{in\omega t} \quad (29b)$$

IV. THERMAL LOAD LEVELING (TLL)

Since solar radiation and ambient air temperature are periodic in nature, the room air temperature will fluctuate. Thermal load leveling (TLL) is used as a measure to indicate this fluctuation and is given as:

$$TLL = \frac{T_{r \max} - T_{r \min}}{T_{r \max} + T_{r \min}} \quad (30)$$

V. DECREMENT FACTOR (F)

The reduction in amplitude of temperature at the inside surface compared to the outside surface of the room is expressed by decrement factor. It is given as (Ozel, 2013):

$$f = \frac{(T|_{x=L})_{\max} - (T|_{x=L})_{\min}}{(T|_{x=0})_{\max} - (T|_{x=0})_{\min}} \quad (31)$$

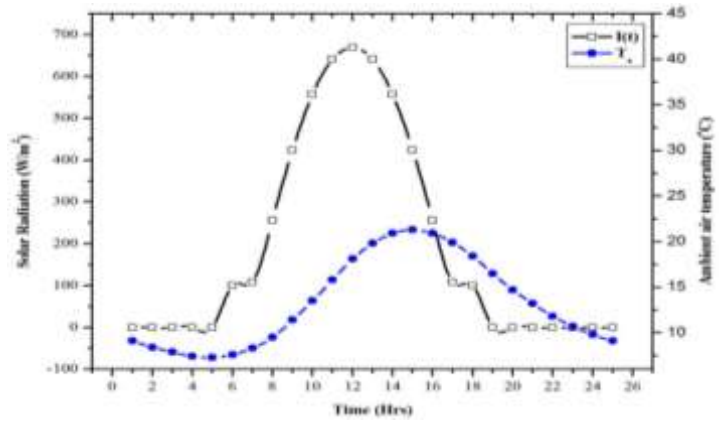


Fig. 4. Hourly variation of solar radiation,  $I(t)$ , and ambient air temperature,  $T_a$ .

VI. OVERALL EXERGY

The rate of thermal energy transferred from the Trombe at  $T|_{x=L}$  and thermal energy arriving from upper vent is given by:



$$\dot{Q}_{\text{uth}} = h_i (T|_{x=L} - T_r) , \text{ and} \quad (32)$$

$$\dot{Q}_{\text{up}} = \dot{m}_f c_f (T_{\text{fout}} - T_r) \quad (33)$$

Therefore, the total rate of thermal energy received by the room is given by:

$$\dot{Q}_{\text{th}} = \dot{Q}_{\text{uth}} + \dot{Q}_{\text{up}} \quad (34)$$

Further, an exergy of thermal energy can be evaluated as:

$$\dot{Q}_{\text{uex}} = h_i \left[ (T|_{x=L} - T_r) - (T_a + 273) \ln \left( \frac{T|_{x=L} + 273}{T_r + 273} \right) \right] \quad (35)$$

$$\dot{Q}_{\text{uex}} = \dot{m}_f c_f \left[ T_{\text{fout}} - T_r - (T_a + 273) \ln \left( \frac{T_{\text{fout}} + 273}{T_r + 273} \right) \right] \quad (36)$$

Electrical exergy, equivalent to electrical energy, can be written as:

$$\dot{E}_{\text{xel}} = \eta_m I(t) A_m \quad (37)$$

Finally, overall exergy can be expressed as the sum of exergy of thermal energy, given by Eqs. (35) - (36), and electrical exergy, (Eq. 37). Overall exergy can be expressed as:

$$\dot{E}_{\text{xov}} = \dot{E}_{\text{xel}} + \dot{Q}_{\text{uex}} \quad (38)$$

## VII. METHODOLOGY

The following methodology has been considered for analysis of SPVT-TW with air duct/vent.

- Hourly variation of solar intensity and ambient air temperature, depicted in Fig. 4, and the design parameters, specified in Table 1, have been used for computations.
- Fourier coefficients for Eqs. (6) and (7) are determined. Subsequently, simulation is performed using MATLAB 2013b software platform.
- Time-independent constants ( $T_{co}$ ,  $A$ ,  $B$ ,  $T_{ro}$ ,  $T_{fo}$ ) (Eq. (27)) and time-dependent constants ( $T_{cn}$ ,  $Cn$ ,  $D_n$ ,  $T_m$ ,  $T_{fn}$ ) (Eq. (29)) are computed using matrix inversion.
- The known constants  $T_r$ ,  $T_c$ ,  $T_f$ ,  $T|_{x=0}$  and  $T|_{x=L}$  are computed.
- Using the numerical value of  $T_c$ , PV module's temperature and electrical energy are evaluated using Eqs. (1) and (37) respectively.

- Eqs. (35)-(36) are used to evaluate the exergy of thermal energy and overall exergy is computed using Eq. (38).

## VIII. RESULTS AND DISCUSSION

After mathematical modeling of the system, simulation is developed using MATLAB 2013b software and the effect of different parameters such as thickness of Trombe wall, absorptivity, packing factor, and transmittivity of PV module on room air temperature and thermal comfort of the room is evaluated.

Fig. 4 shows the hourly variation of solar intensity and ambient air temperature as measured on January 21<sup>st</sup>, for New Delhi, India. Fig. 5a depicts the room air temperature, temperature distribution at  $x=0$  (outer surface of Trombe wall, painted black) and temperature distribution at  $x=L$  (i.e. inner surface of Trombe wall) for different thickness of Trombe wall, for vented SPVT-TW.

It can be seen that the fluctuation in room air temperature decreases with an increase in thickness of Trombe wall, and it maintains at around 45 °C. Fig. 5b compares the hourly variation of room air temperature of vented SPVT-TW with SPVTW without vent (Taffesse et. al., 2016) for different Trombe wall thicknesses. It can be seen from Fig. 5b that the room air temperature for vented SPVT-TW is higher than for SPVT-TW without vent. Also, the vented SPVT-TW gives better thermal stability in room, with less thickness of Trombe wall, than the SPVT-TW without vent. Further, it can be observed that for higher thickness of Trombe wall, room air temperature and  $T|_{x=L}$  are the same for vented SPVT-TW (Fig. 5a), as expected.

Fig. 6 demonstrates the comparison between thermal load leveling for the SPVT-TW with and without vent. The SPVT-TW with vent achieves better thermal stability or less fluctuation in room air temperature than the SPVT-TW without vent (Taffesse et. al., 2016). The vented SPVT-TW provides better thermal comfort with small thickness of Trombe wall as compared to the SPVT-TW without vent. The optimum thickness of Trombe wall, which offers higher stability of room air temperature for vented and unvented SPVT-TW, is 0.3 m and 0.4 m respectively.

Fig. 7 illustrates the effect of mass flow rate on cell temperature (a) and electrical efficiency of PV module (b). It can be seen that the solar cell temperature increases as the mass flow rate decreases and hence, the electrical efficiency decreases as expected. However, the room air temperature will decrease with a decrease in mass flow rate.

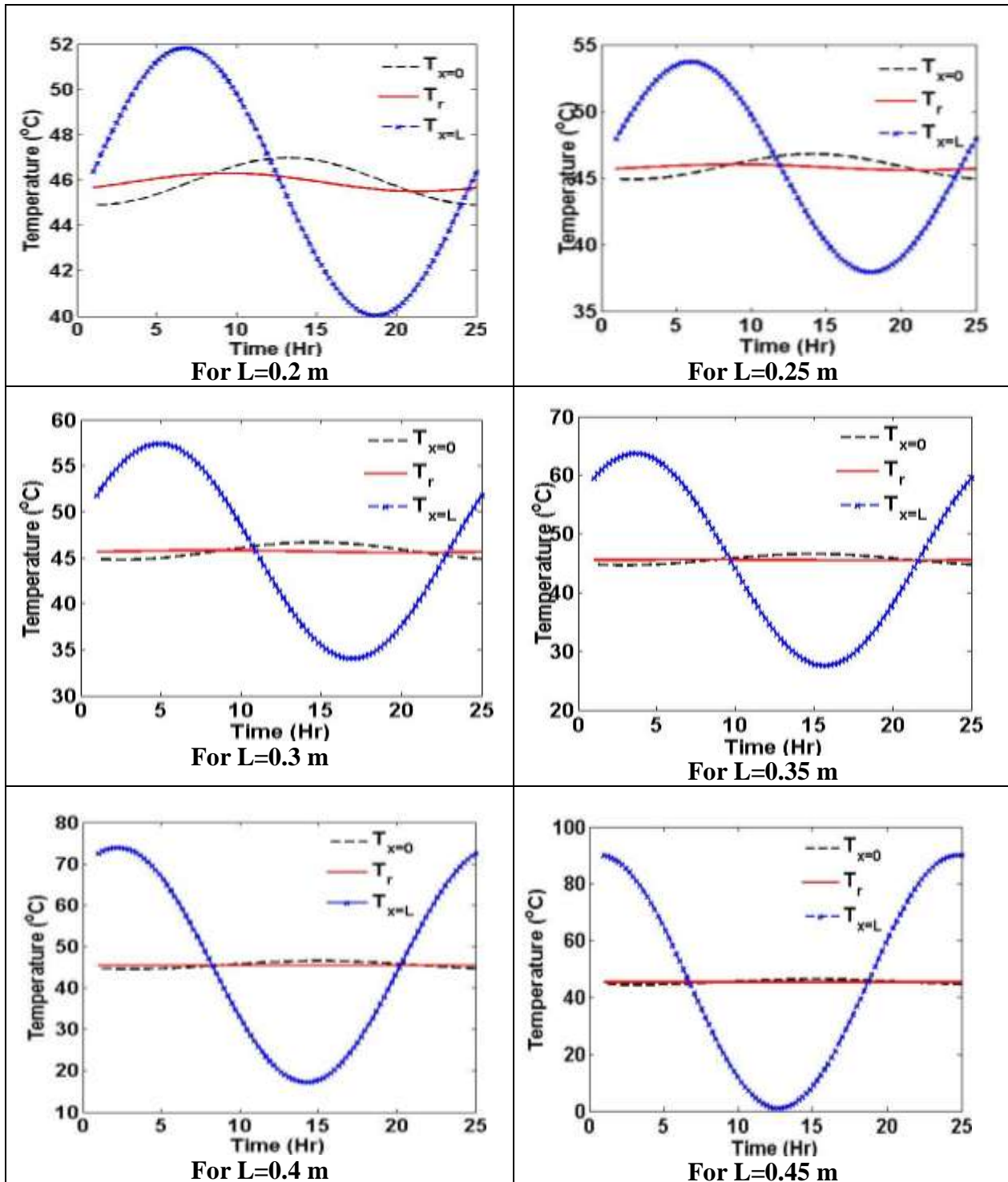


Fig. 5a. Hourly temperature distribution for Trombe wall at  $T_{x=0}$ ,  $T_{x=L}$  and room air temperature,  $T_r$ .

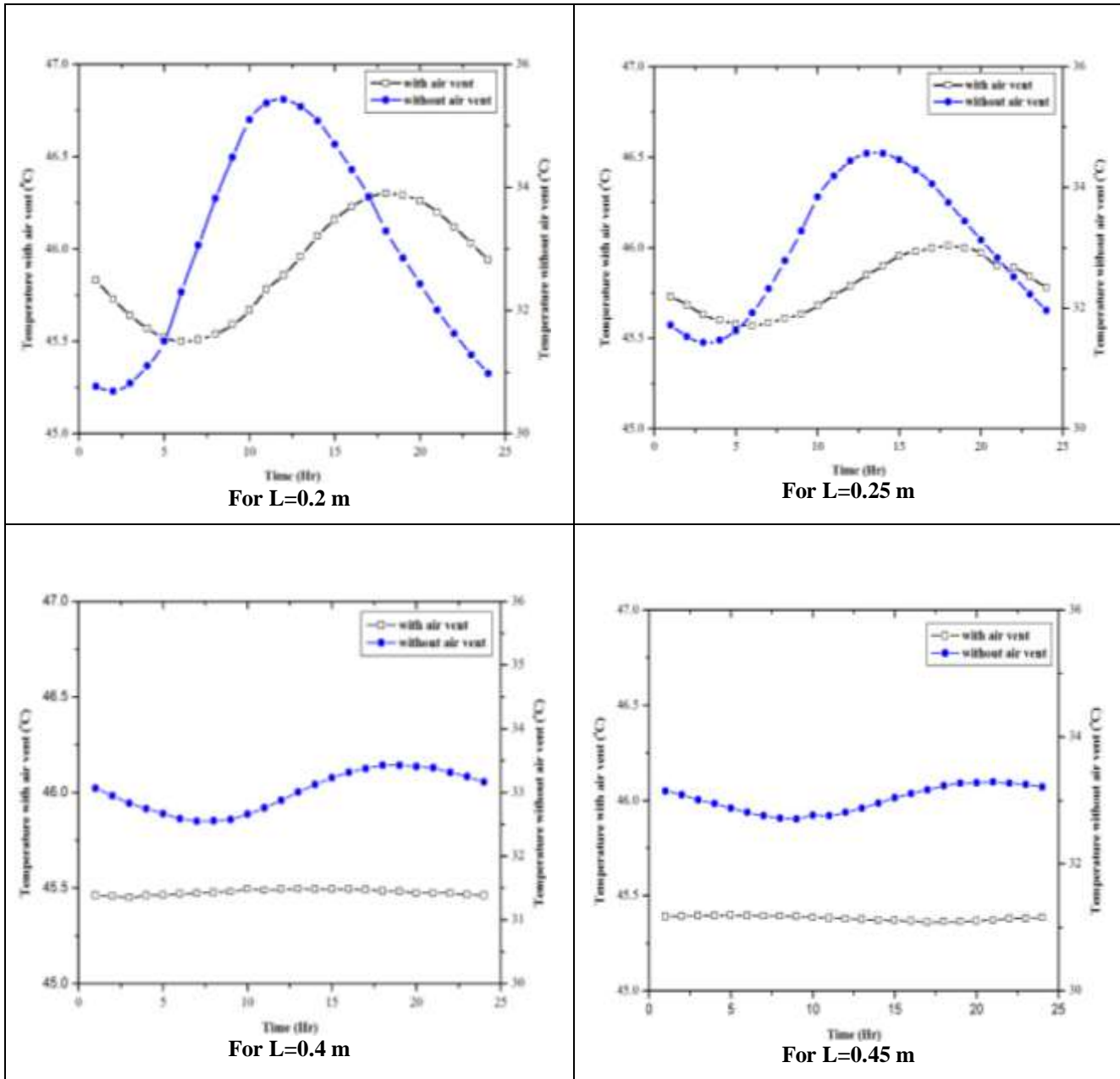


Fig. 5b. Hourly room air temperature distribution for different thicknesses of Trombe wall in SPVT-TW with and without air vent.

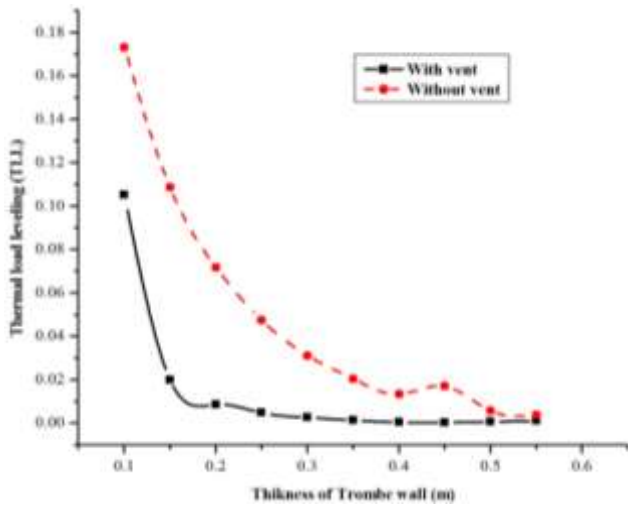


Fig. 6. Variation of thermal load leveling with thickness of Trombe wall.

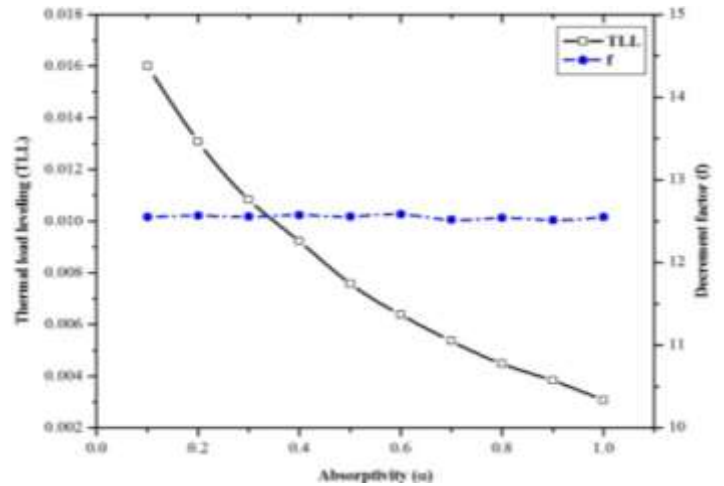


Fig. 8. Variation of thermal load leveling and decrement factor with absorptivity of PV module.

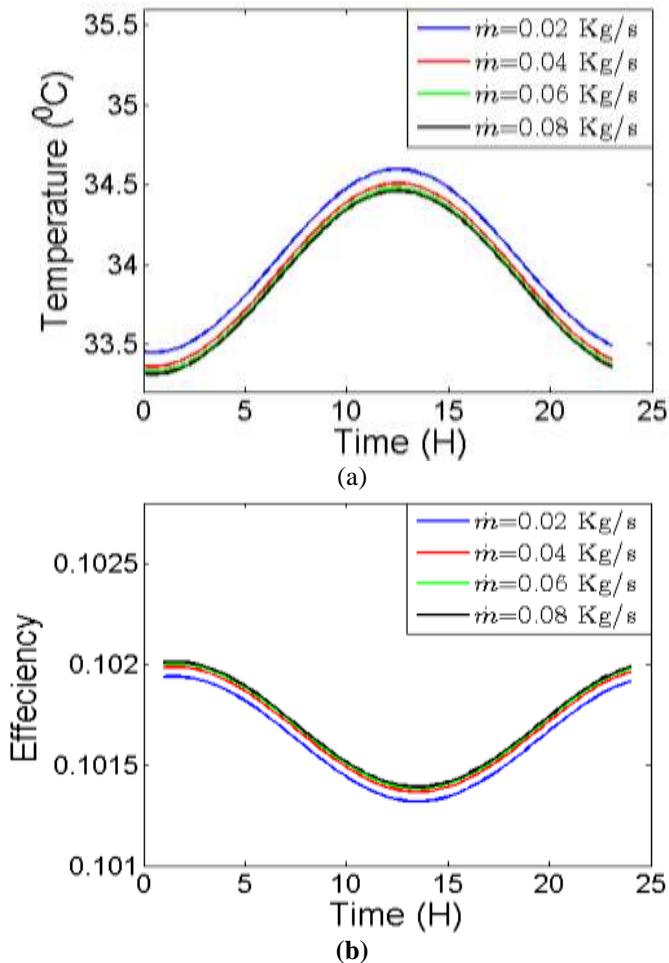


Fig. 7. Hourly variation of (a) cell temperature with mass flow rate and (b) efficiency of PV module with mass flow rate

Fig. 8 illustrates the variation in absorptivity of PV module with thermal load leveling and decrement factor. As can be seen, with an increase in absorptivity of PV module, there is a decrease in thermal load leveling and consequently, a better thermal stability is achieved inside the room. From thermal point of view, the optimum value of TLL is obtained as 0.0037 for absorptivity 0.9.

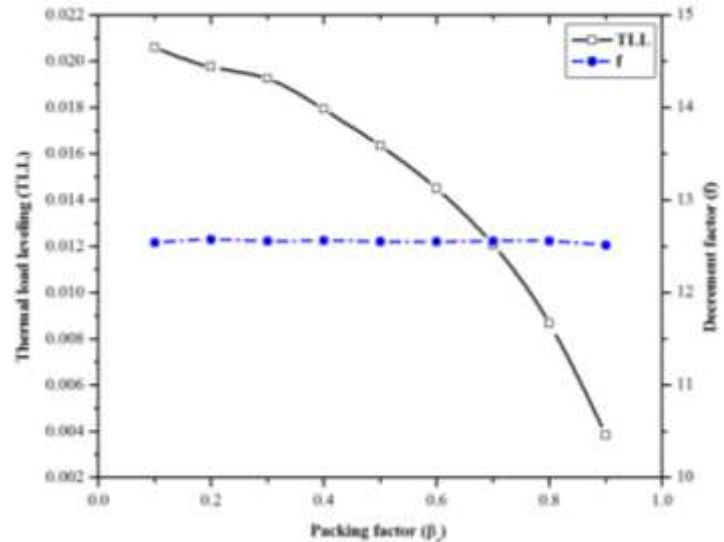


Fig. 9. Variation of thermal load leveling and decrement factor with packing factor of PV module.

Fig. 9 depicts the effect of packing factor of the PV module on thermal load leveling and decrement factor. As the packing factor increases, a better thermal load leveling, as



well as decrement factor, are attained. The optimum value of TLL is obtained as 0.0038 for a packing factor of 0.9. Therefore, for a better thermal stability in the room, a higher packing factor is preferable.

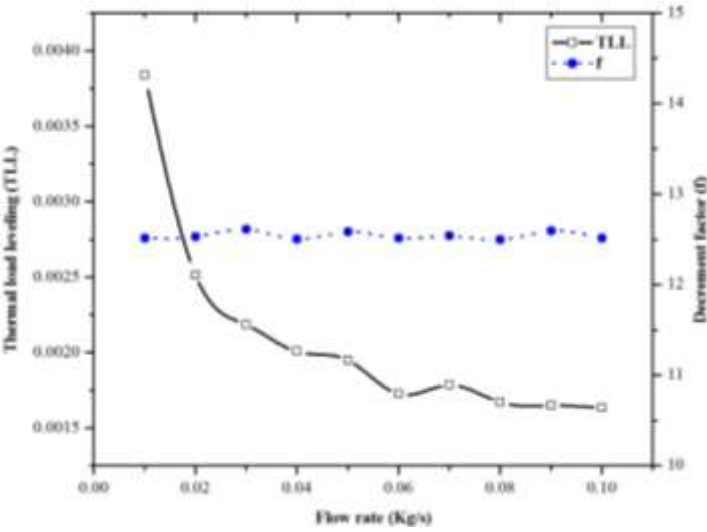


Fig. 10. Variation of thermal load leveling and decrement factor with mass flow rate of air.

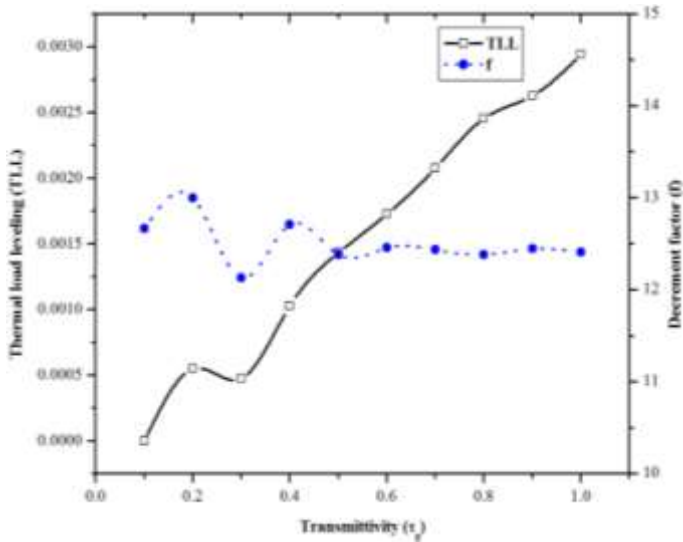


Fig. 11. Variation of thermal load leveling and decrement factor with transmittivity of PV module.

Fig. 10 illustrates the effect of mass flow rate on the thermal stability of the room. It can be seen that for a better room air temperature stability, the mass flow rate should be high. Hence, by controlling the mass flow rate of air we can provide a better thermal comfort to the room. By

considering the cost and size of the fan, the optimum value of mass flow rate should be 0.06 Kg/s, for which TLL is 0.0017.

The effect of transmittivity on thermal stability inside a room is shown in Fig. 11. As can be seen, an increase in transmittivity causes the thermal load leveling to increase. From a thermal comfort point of view, the thermal load leveling should be as low as possible and this can be achieved by considering a low value of transmittivity. Therefore, the optimum value of transmittivity is 0.4, for which thermal load leveling is 0.00208.

The variation of an exergy of thermal energy, electrical energy, and an overall exergy are given in Fig. 12. As shown, the rate of thermal exergy is much lower than electrical output, as expected. This indicates that the vented SPVT-TW can provide electrical power in addition to the thermal needs of a building.

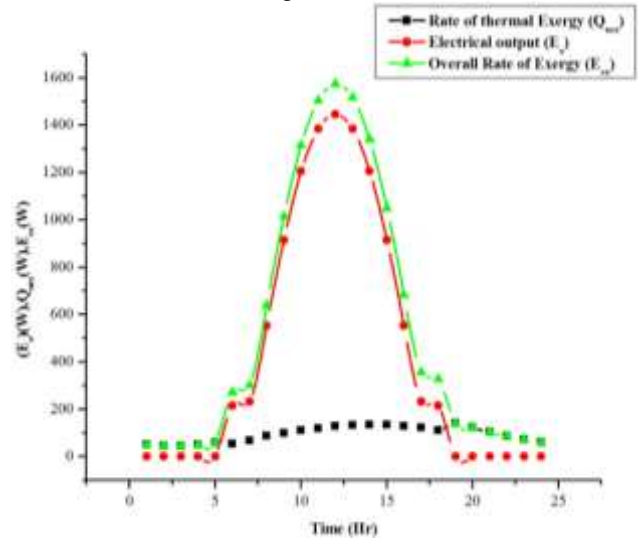


Fig. 12. Hourly variation of rate of thermal exergy, electrical output and an overall exergy.

## IX. CONCLUSIONS

- The effect of thickness of Trombe wall on room air temperature has been analyzed and consequently, the optimum thickness of Trombe wall for vented SPVT-TW is obtained to be 0.3 m for comfortable room air condition.
- The mass flow rate of air has a noteworthy influence on room temperature as well as thermal stability within the room. In order to achieve a better thermal stability in the room, the mass flow rate should be 0.06 Kg/s and the corresponding thermal load leveling is 0.0017.
- Vented SPVT-TW can provide more heat energy to the room and thus, the room air temperature is



higher for vented SPVT-TW than for SPVT-TW without vent. (Taffesse et. al., 2016), with the difference being around 10-12 °C.

- The design parameters like packing factor, transmittivity and absorptivity of PV module have a significant effect on thermal stability inside the room. From the analysis, the ideal values of transmittivity, absorptivity and packing factor are obtained as 0.4, 0.9 and 0.9 respectively, with the corresponding thermal load leveling of 0.0038, 0.000208 and 0.0037 respectively.

#### X. RECOMMENDATIONS

- Experimental validation should be carried out for the proposed thermal model for different climatic conditions.
- The proposed model could be extended for thermal cooling for hot climatic conditions.

| Design Parameters  |  |
|--|--|
| $w = \frac{2\pi}{24} \text{ (rad h}^{-1}\text{)}$          | $A_m = 20 \text{ m}^2$                                 |
| $w_o = \frac{2\pi}{24 * 3600} \text{ (rad s}^{-1}\text{)}$ | $M_a = 147 \text{ Kg}$                                 |
| $c = 0.84 \text{ (KJ/Kg K)}$                               | $C_a = 1.005 \text{ (KJ Kg}^{-1}\text{K}^{-1}\text{)}$ |
| $\rho = 1600 \text{ (Kg/m}^3\text{)}$                      | $u_t = 5.54 \text{ (W/m}^2\text{)}$                    |
| $\tau_g = 0.9$   | $u_b = 2.8 \text{ (W/m}^2\text{)}$                     |
| $L_g = 0.003 \text{ m}$                                    | $\alpha_c = 0.9$                                       |
| $K_g = 0.6 \text{ W/m}$                                    | $\alpha_{bb} = 0.9$                                    |
| $K = 0.69 \text{ (W/m K)}$                                 | $\beta = 0.9$  |
| $h_i = 2.8 \text{ (W/m}^2 \text{ K)}$                      | $\beta_o = 0.0045 \text{ (K}^{-1}\text{)}$             |
| $h_o = 5.54 \text{ (W/m}^2 \text{ K)}$                     | $b = 0.15 \text{ m}$                                   |
| $A_r = 30 \text{ m}^2$                                     | $L_o = 3 \text{ m}$                                    |
| $\eta_{co} = 0.12$   | $\eta_{co} = 0.12$                                     |
|  | $h_{bf} = 18 \text{ (W/m}^2 \text{ K)}$                |

Table 1. Various design and specification parameters used for SPVT-TW with air duct/vent.

Table 2. Nomenclature

|  |   |   |
|--|---|---|
| $A_m$ PV module's area ( $\text{m}^2$ )                              | $h_i$ convective and radiative heat transfer coefficient from internal surface of Trombe wall to room ( $\text{W/m}^2 \text{ K}$ )      | surface of Trombe wall through glass cover ( $\text{W/m}^2 \text{ K}$ ) |
| $A_r$ area of single room ( $\text{m}^2$ )                           | $h_{bf}$ convective heat transfer coefficient from blackened surface of Trombe wall to air inside the duct ( $\text{W/m}^2 \text{ K}$ ) | <b>Greek symbols</b>  |
| $C_a$ specific heat of air ( $\text{J/Kg } ^\circ\text{C}$ )         | $T_a$ ambient temperature ( $^\circ\text{C}$ )  | $\alpha_c$ absorptivity of solar cell                                   |
| $M_a$ mass of air (Kg)   | $T_c$ solar cell temperature ( $^\circ\text{C}$ )   | $\alpha_{bb}$ absorptivity of blackened surface of Trombe wall.         |
| $\dot{m}_f$ mass flow rate of air ( $\text{Kg/s}$ )                  | $T_r$ room air temperature ( $^\circ\text{C}$ )   | $\beta$ packing factor of PV module                                     |
| $b$ gap between the PV module and Trombe wall (m)                    | $V_a$ speed of air (m/s)  | $\beta_o$ temperature coefficient ( $\text{K}^{-1}$ )                   |
| $L$ thickness of Trombe wall (m)                                     | $U_t$ overall heat transfer coefficient from solar cell to ambient through glass cover ( $\text{W/m}^2 \text{ K}$ )                     | $\eta_m$ efficiency of PV module  |
| $L_o$ height of Trombe wall (m)                                      | $U_b$ overall heat transfer coefficient from solar cell to blackened  | $\rho$ density of concrete (stone) ( $\text{Kg/m}^3$ )                  |
| $I(t)$ solar radiation ( $\text{W/m}^2$ )                            |   | $\tau_g$ transmittivity of glass  |
| $K$ thermal conductivity ( $\text{W/m K}$ )                          |   | $\eta_{co}$ efficiency of PV cell at standard test condition            |
| $L_g$ thickness of glass (m)   |   | <b>subscripts</b>   |
| $K_g$ thermal conductivity of glass ( $\text{W/m K}$ )               |   | m module, t top, r room, a air  |
| $n$ number of harmonics  |   | c solar cell, g glass, b bottom   |
| $h_o$ outside heat transfer coefficient ( $\text{W/m}^2 \text{ K}$ ) |   | bb blackened  |



## XI. REFERENCES

- [1] Gan, G., 1998. A parametric study of Trombe walls for passive cooling of buildings. *Energy and building* 27, 37-43.
- [2] Irshad, K., Habib, K., Thirumalaiswamy, N., 2015. Performance Evaluation of PV-Trombe Wall for Sustainable Building Development. 12th Global conference on sustainable manufacturing procedia CIRP. 26, 624-629.
- [3] Jiang, B., Jie, J., Hua, Y., 2008. The influence of PV coverage ratio on thermal and electrical performance of photovoltaic-Trombe wall. *Renewable energy* 33, 2491-2498.
- [4] Jie, J., Hua, Y., Wei, H., Gang, P., Jianping, L., Bin, J., 2007. Modeling of a novel Trombe wall with PV cells. *Building and Environment* 42, 1544-1552.
- [5] Koyunbaba, B.K., Yilmaz, Z., 2012. The comparison of Trombe wall systems with single glass, double glass and PV panels. *Renewable Energy* 45, 111-118.
- [6] Mansour A.R., Jubran, B.A., Tashtoush, B., 1991. An approximate analytical solution to convective laminar heat transfer flow within the trombe wall channel. *International Communications in Heat and Mass Transfer* 18, 153-159.
- [7] Ozel, M., 2013. Determination of optimum insulation thickness based on cooling transmission load for building walls in a hot climate. *Energy Conversion Management* 66, 106-114.
- [8] Rabani, M., Kalantar, V., Dehghan, A.A., Faghih, A.K., 2015. Experimental study of the heating performance of a Trombe wall with a new design. *Solar Energy* 118, 359-374.
- [9] Smolec, W., Thomas, A., 1991. Some aspects of trombe wall heat transfer models. *Energy Conversion Management* 32, 269-277.
- [10] Taffesse, F., Verma, A., Singh, S., Tiwari, G.N., 2016. Periodic modeling of the semi-transparent photovoltaic thermal-Trombe wall (SPVT-TW). *Solar Energy* 135, 265-273.